Introduction of a New Suction based Dielectric Flushing in Reverse-µEDM

WCMNM 2021

Hreetabh Kishore[1], Vikrant Sharma[2], Jay Airao[1], Chandrakant K Nirala[1], Anupam Agrawal[1]
[1]Department of Mechanical Engineering, Indian Institute of Technology Ropar, Rupnagar, (Pb), India-140001.
[2]Department of Mechanical Engineering, CCET Chandigarh, (UT), India-160019.

Abstract

Debris accumulation in tiny discharge gap of micro-electro-discharge machining (µEDM) is attributed to frequent abnormal pulse discharges. As a result, the material removal rate, surface quality and dimensional accuracy in the fabrication of 3D micro components decline. The consequences happen to be more severe while fabricating an arrayed protruding microstructure using Reverse-µEDM. An effective flushing of the debris may lead to healthier discharge pulses and accurate machining responses. The present work demonstrates an innovative strategy to improve the material removal rate (MRR) by incorporating forced flushing as a novel high-pressure suction technology in Reverse-µEDM. A discrete phase flow-field computational model-based analysis on debris ejection mechanism using suction flushing has been presented and validated through experiments. Debris ejection mechanism has been analyzed under different suction pressure while fabricating arrayed protruding microstructures of droplet cross-section. The MRR was enhanced by approximately 25% upon incorporating the developed flushing technology successfully, demonstrating an improved debris ejection strategy from the discharge gap.

1. Introduction

The tremendous potential of Reverse-µEDM is the ability to fabricate protruded structures of high aspect ratio irrespective of the hardness of the conductive material [1]. However, abnormal discharges, including frequent short-circuiting, are always a drawback of the process. The frequent short-circuiting is due to insufficient flushing of the debris accumulated in the narrow discharge gap between the workpiece and the Tool-plate, preventing healthy discharges from occurring. The debris particles are mainly spherical, having a diameter in the range of 90-180 nm [2], an effective evacuation of which becomes problematic in normal conditions in which the dielectric is generally kept stagnant. A more serious concern of improper debris evacuation is observed in Reverse-µEDM while fabricating arrayed protruded microstructures, especially in the case of a dense array with high aspect ratio structures [3]. A frequent short-circuiting caused by the debris accumulation limits the recommended minimum thickness and inter-pre-drilled hole of the Tool-plate [4]. Error-free protruded structures are anticipated to be implemented as micro pin-fins for the thermal management of microelectronic devices. The dimensional accuracies and the surface quality of the fabricated pin-fins are of major concern in such applications.

Moreover, unexpectedly a longer machining time and distorted edges of the pins are few other significant issues encountered. Among the major challenges, increasing the MRR and reducing the edge distortion are given prime importance [3]. It is well understood that to get rid of the issues faced, It is essential to have control over the flushing of the accumulated debris in the discharge gap.

Several effective flushing strategies, such as jet flushing [5], internal flushing [6], and spray flushing [7] proposed earlier, are limited to only conventional straight polarity EDM processes. Recently, Mastud et al. [2] have presented a 2D debris flow field model in vibration-assisted Reverse-µEDM. They quantified the effective debris ejection behavior at different frequencies and amplitude of electrode vibration. Besides, the successful debris evacuation directly from the discharge gap is still a challenging task once the workpiece electrode has progressed to a particular depth. It may obstruct Reverse-µEDM application for high aspect ratio arrayed protruded microstructures.

In this regard, a novel suction flushing strategy has been introduced for Reverse-µEDM, which could evacuate debris rapidly from the discharge gap. This flushing strategy is implemented to Reverse-µEDM simultaneously to the inbuilt dielectric circulation mechanism. High-pressure suction-assisted flushing takes place from the backside of the pre-drilled Tool-plate. Based on the reviews of the relevant literature, it has been found that in Reverse-µEDM, the issue of insufficient debris flushing from the tiny discharge gap remains un-attempted.

The present work introduces a novel high-pressure suction-assisted flushing technology. A discrete phase flow-field computational model-based analysis on debris ejection mechanism using suction flushing has been presented. The flow patterns of ejected debris have been analyzed for providing insight into the debris flow behavior in suction flushing using ANSYS®-Fluent CFD solver. Furthermore, experimental validation of the developed model has been performed using an in-house developed suction flushing setup. An array of protruded microstructures in droplet cross-section, which has a certain advantage over other regular shapes such as circular and square [8], have been fabricated. The benefits of the suction-assisted flushing technique have been evidenced through a comparative analysis.

2. High-pressure suction flushing technology

Concerning the inherent issues of debris accumulation and insufficient evacuation at a narrow discharge gap in the Reverse-µEDM, initially, a single micro protruded structure has been fabricated. The image of debris accumulation at the narrow discharge gap is captured using high-speed imaging confrontation (Make: FastCam SA4, Photron, 3600 fps) as shown in Fig. 1. The ejected debris tries to splash out of the discharge gap or float on the Tool-plate's surface. The presence of debris for a long-time has always been a drawback of the process. However, the severity of the poor flushing is more prominent at the central portion of the workpiece during the fabrication of arrayed protruded microstructures of irregular cross-section profiles.

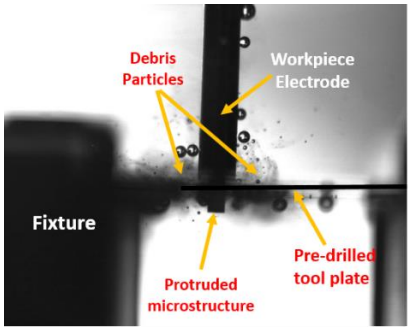

Fig. 1. Illustration of debris ejected during Reverse-µEDM of single micro-pin.

The schematic of hybridized microfabrication setup for such fabrication is shown in Fig. 2(i) and (ii).
The high-pressure suction flushing technology is a simultaneous application to the Reverse-µEDM, due to which the drawbacks of debris accumulation at the machining area and longer machining time are supposed to be overcome. The performances of developed suction flushing have been evaluated through computational modeling followed by experimental pilot runs for validation, as discussed in section 3.

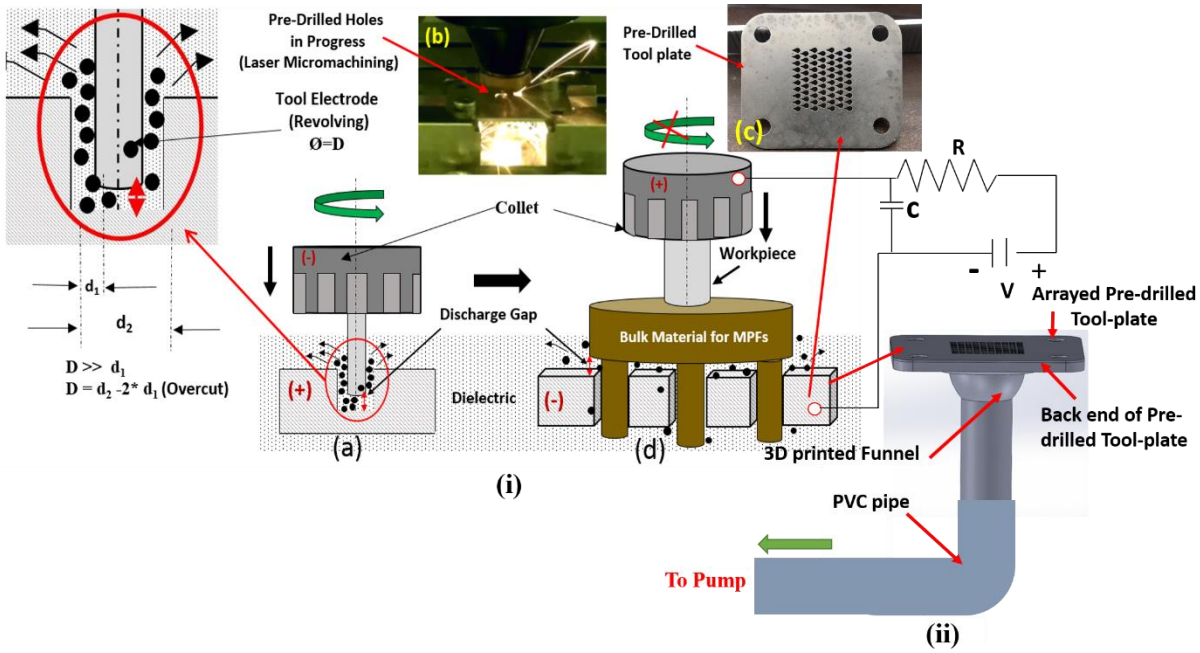

Fig. 2. (i) Schematic illustration of (a) µEDM drilling (b) Reverse-µEDM process by reversing the polarity of (a), (c) arrayed pre-drilled holes for Reverse-µEDM, (d) LASER micromachining for fabricating pre-drilled Tool-plate, and (ii) suction flushing technology setup.

3. Formulation of the numerical model

The workpiece and the pre-drilled tool plate electrodes, and the suction flushing setup, are submerged in the dielectric pool during the Reverse-µEDM. However, it is more challenging to capture the motion of debris during experimentation. Therefore, we attempted to simulate a real-time suction flushing model to analyze the accretion, distribution and ejection trajectory of debris. In this regard, the 2D simulations have been performed considering the necessary boundary conditions and assumptions.
In the model, each side of the workpiece electrode is 10 mm, with the initial discharge gap between the workpiece and Tool-plate electrodes is five µm. The pre-drilled Tool-plate and the workpiece material are assigned as solid material. Ejection of solid spherical-shaped debris is allocated from the workpiece frontal surface towards the lower side. The material of ejected debris (nano-size) is assigned as yellow brass. The present simulation uses debris with a dia. of 4µm, a mass of 2.87×10^{-13}kg, and a density of 8730 kg/m^3. Debris injected in the discharge gap with an injection velocity of 1.25 m/s and a flow rate of 0.0001 kg/s towards the pre-drilled Tool-plate. A continuous fresh dielectric fluid flow at pressurized flushing conditions with a velocity of 0.02m/sec was applied at the inlet as shown in Fig. 3. It is assumed that the

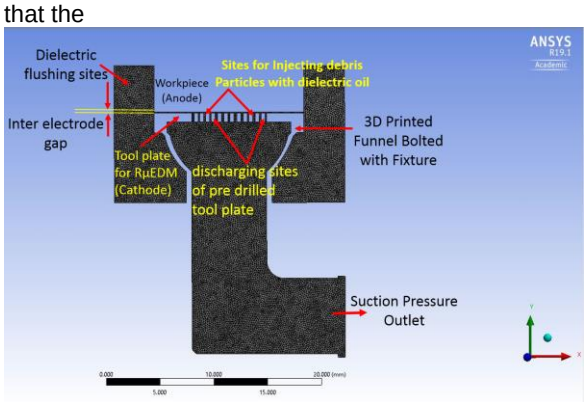

Fig. 3. Detailed pictograph of Computational domain with Boundary conditions for suction-assisted flushing technology in Reverse-µEDM process.

liquid dielectric has homogenous, isotropic, and incompressible fluid properties. The dielectric oil mixed with debris leaves the machining area through the suction funnel outlet with a back pressure less than atmospheric pressure. The total time step to run a simulation is approximately 8000 sec with an incremental step time of $3\text{x}10^{-5}$ sec. A fine-structured triangular mesh is used to generate the numerical model, followed by several grid independence tests to find the computational model with a higher

convergence rate. A relatively fine mesh with a maximum number of 26,364 nodes is adopted for the fluid domain to capture debris behavior. The model, along with the respective boundary conditions, is presented in Fig. 3.

In the simulation, the debris particle exchanges its mass, momentum, and energy with the dielectric fluid. The inlet is maintained at the atmospheric condition, and the outlet is given a negative back-pressure boundary condition. The fluid flow phenomena, represented by Eq. 1, is integrated over each controlled volume in the computational domain [9]:

$$\frac{\partial}{\partial t}(\rho\phi) + \frac{\partial}{\partial x_i}(\rho u_i \phi) - \frac{\partial}{\partial x_i}\left[\Gamma_\phi \frac{\partial \phi}{\partial x_i}\right] = S_\phi \quad (1)$$

where (ρ) is a fluid density, (Γ_ϕ) is a diffusion coefficient for (ϕ) and (S_ϕ) is a source term. The mass (Eq. 2) and momentum conservation (Eq. 3) equations are used to demonstrate the fluids flow behaviour. For continuity equation ϕ = 1 whereas, Γ_ϕ and S_ϕ are zero in Eq. 1. For the momentum conservation equation, the transported variable, u_i is velocity, Γ_ϕ is viscosity and S_ϕ represents the sum of the forces acting on the fluid [10]:

$$\frac{\partial \rho}{\partial t} + \frac{\partial}{\partial x_i}(\rho u_i) = 0 \quad (2)$$

$$\frac{\partial}{\partial t}(\rho u_i) + \frac{\partial}{\partial x_i} = -\frac{\partial P}{\partial x_i} + \frac{\partial}{\partial x_j}\left[\mu\left(\frac{\partial u_i}{\partial x_j} + \frac{\partial u_j}{\partial x_i}\right)\right] \quad (3)$$

where (t) is the time, (u) is the velocity of fluid flow, subscript (i,j) is designated as the Cartesian coordinates of fluid flow velocity components, (x) is coordinate, and (μ) is fluid viscosity. On the left-hand side of Eq.3, the first term represents the temporal variation of momentum and the second term represents the downstream fluid's acceleration. Consequently, the right-hand terms represent resultant forces such as pressure gradient force (normal stresses) and viscous force (tangential shear stresses).

In the computational domain, less than 10% volume of the debris in the total fluid phase is considered. Debris particle trajectories along the tertiary phase have been evaluated by integrating the force-balance equation coupled with the Eulerian-Lagrangian frame. The relation given in Eq. 4 evaluates the debris inertia and the drag force acting on the primary phase debris. a

$$\frac{du_p}{dt} = F_D\left(\vec{u} - \overrightarrow{u_p}\right) + \frac{\vec{g}\,(\rho_p - \rho)}{\rho_p} + \vec{F} \quad (4)$$

where, ($\frac{du_p}{dt}$) is the net inertia of the particle, ($\vec{g}$) is the gravity force, (F_D) is the drag force and ($\vec{F}$) is the additional force as source terms. This force is raised due to the pressure gradient of the fluid flow in the domain.

$$F = \left(\frac{\rho}{\rho_p}\right)\underset{u_p}{\rightarrow}\frac{du}{dx} \quad (5)$$

Additionally, the detailed drag force equation is given by Eq. 6:

$$F_D = \frac{18\mu C_D R_E}{24\rho_p d_p^2} \quad (6)$$

Where ($\overrightarrow{u}$) is the dielectric fluid velocity, ($\overrightarrow{u_p}$) is the velocity of the debris, (μ) is the dynamic viscosity of the dielectric fluid, (ρ) is the density of the dielectric fluid, (ρ_p) is the density of the debris in the dielectric fluid, (d_p) is the diameter of debris and (Re) is the Reynolds number as given by Eq. 7:

$$Re = \frac{\rho d_p \left|\overrightarrow{u_p} - \vec{u}\right|}{\mu} \quad (7)$$

In the present work, the debris has been considered to be spherical in shape; hence, the drag coefficient is also considered for a smooth motion of the debris as given in Eq. 8 [10]:

$$C_D = a_1 + \frac{a_2}{R_E} + \frac{a_3}{R_E^2} \quad (8)$$

where, (a_1, a_2, a_3) are the constants applied for a specific range of Reynolds number.

By integrating Eq. 4 with time yields the velocity of the debris at each point along the trajectory, with the trajectory itself predicted by Eq. 9:

$$\frac{dx_p}{dt} = u_p \quad (9)$$

Both the Eqs. 4 and 9 were solved for coordinate direction for predicting debris trajectories in the discrete phase.

Further, the model is subjected to discrete phase modelling (DPM) for studying the debris particle's behavior. In this method, the primary and secondary phases are considered dielectric liquid (fluid domain), and the tertiary phase is considered injected solid debris. Primary and secondary phases have been solved using Navier-Stokes equations, and the tertiary phase is solved using the Eulerian-Lagrangian approach. The DPM model consists of four different boundary conditions: reflect, trap, escape, and wall jet. The reflect boundary condition applies when the ejected debris particle hits the Tool-plate surface and rebounds by changing its momentum and direction, where the holes are not present. The escape boundary condition applies during the debris path gets terminated in the trap when it touches the sidewall of holes.

Additionally, the number of debris trapped or escaped at the discharge gap from the pre-drilled holes is then calculated. Moreover, escape boundary conditions have been assigned at the outlet to prevent the back reflection of the debris. The wall jet condition is applied on the workpiece frontal surface. The remaining walls of the computational domain are considered as reflection boundary conditions. The realizable k–ε model with enhanced wall functions is used to track the debris ejection in this simulation. This model is also used to capture localized turbulency or vortex formation at the back-end of the pre-drilled Tool-plate. The SIMPLE algorithm is considered for the discretization of pressure-velocity coupling equations. Therefore, transient-based debris particle tracking with well-known spherical drag law is deemed to follow the debris in the fluid domain.

4. Experimental setup

In the suction flushing setup, the flushing occurs from the back-end of the pre-drilled tool-plate anticipating a significant improvement in the output responses. The realistic technology setup of novel high-pressure suction flushing is shown in Fig. 4. A similar suction-based flushing approach was adopted by Kishore et al. [11] for enhancing product quality and MRR and by Tanjilul et al. [4] for enhancing the surface quality and reducing the machining time. Three-axis Multipurpose hybrid µEDM machine (make: MIKROTOOLS Pte Ltd., model: DT110i) consisting of a LASER head (for fabricating Tool-plate) has been used to perform experimental runs. Kishore et al. used a similar setup configuration for the fabrication of tool plates for Reverse-µEDM [12]. Different machining conditions

used in the experiment are listed in Table 1. The workpiece and Tool-plate electrodes have been dipped inside a transparent µEDM tank filled with hydrocarbon-based dielectric oil (NICUT LL21 E EDM oil). An inbuilt nozzle-based flushing outlet is used to supply fresh dielectric oil in the tank (shown in Fig.4). A 3D printed funnel is clamped with the pre-drilled Tool-plate (shown in Fig. 4). A 3D printed funnel clamped with the pre-drilled Tool-plate (shown in Fig. 4), ensures no leakage of dielectric oil from the contact surface. The other end of the funnel is connected with the outlet of the self-priming type centrifugal pump as shown in Fig. 4(c).

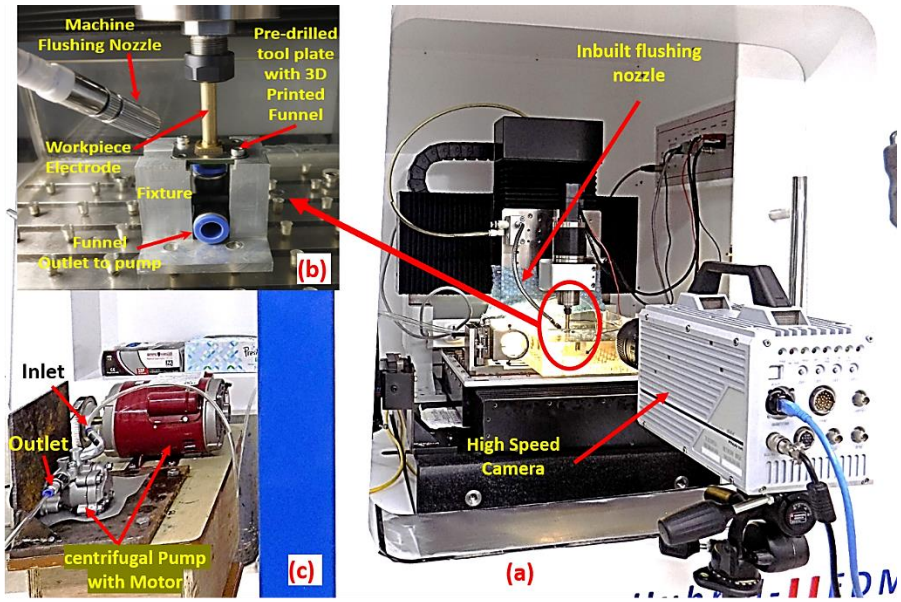

Fig. 4. Experimental setup of developed suction flushing technology in Reverse-µEDM process.

The maximum flow rate of up to 7 L/min through a centrifugal pump rated for a pumping pressure of 0.6 MPa is achieved. A dedicated fixture has been used to hold the pre-drilled Tool-plate. The experimental runs have been performed in two different conditions i.e., with and without the suction flushing technology.

Table 1: Machining Conditions

Reverse-µEDM process parameters	**LASER Micromachining parameters**
Setup - RC based	**LASER type** - Nd-YAG YLR-150/1500-QCW-MM-AC-Y11
Resolution (X, Y, Z) - 0.1µm	**Wavelength** - 1070nm
Tool-plate – Titanium (0.5 mm thick)	**Power** - 150W
Workpiece - Yellow brass	**Frequency** – 50 Hz
Gap Voltage – 110 V	**Pulse width** - 0.5 ms
Capacitance – 100 nF	**Spot dia.** – 55 µm
Electrode feed rate – 10 µm/s	**Current (%)** – 20

5. Results and Discussion

For studying the debris flow trajectory, particles are injected from the frontal surface of the workpiece electrode in the fluid domain. During the suction flushing, the debris experiences several flow behaviors while going downside in the liquid dielectric, such as (i) accretion on the workpiece and Tool-plate surface, (ii) formation of a chain-like cluster of debris, (iii) vortex formation along the sidewall towards the back-end of the Tool-plate (iv) particle ejection trajectory at the funnel outlet. The debris movements at different positions and time steps are recorded as shown in Fig. 5(a)-(f). From Fig. 5, it is observed that most of the ejected debris gets flushed away through pre-drilled holes due to plasma implosion and high suction pressure. The trajectory of debris is computed through the fluid domain over a large number of steps when it passes through the Tool-plate. A change in trajectory length of the debris is observed in the fluid domain. This is attributed to larger fluid velocity and pressure variation across the discharge gap towards the Tool-plate. The overall trajectory of the debris flow has been determined by computing the force balance acting on it and the debris transport assumptions in the flow field domain.

The dynamic nature of debris movement results in a reduction of debris concentration at the localized zone. Whereas the absence of debris reduces a frequent short-circuit and enables a linear motion of the spindle in the negative z-direction. Ultimately it leads to normalizing the discharging and enhances the amount of material removed. It can also be visualized that after implementing high-pressure suction flushing, a minimal amount of debris has adhered at the discharge gap. Simultaneously, it gets flushed out by the pressure of the inbuilt machine flushing. A large concentration of debris gets collected at the funnel outlet, which is further collected back in the EDM tank. Thus the cycle of debris ejection, collection and filtration are continuous for the whole machining time.

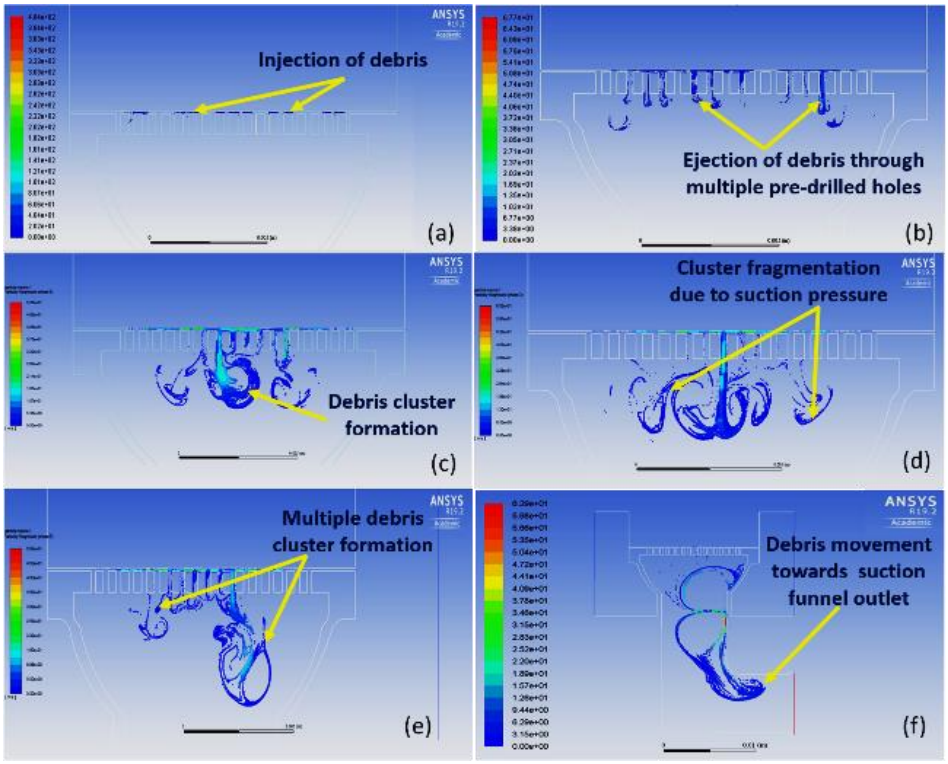

Fig. 5. Debris particle trajectory in suction-assisted flushing technology at different time steps.

Pilot experimental runs have been performed to validate the developed suction flushing model. However, the fabricated protruded microstructures cross-sectional profile is a duplication of the fabricated pre-drilled through holes on the Tool-plate. An array of 7x10 droplet cross-section protruded microstructures in the staggered arrangement was fabricated with and without suction flushing.

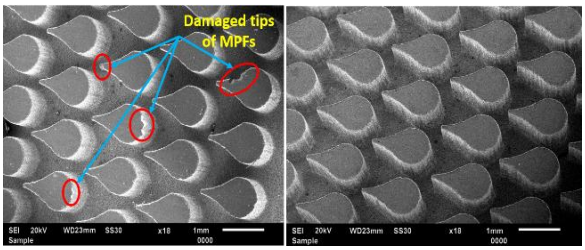

Fig. 6. SEM image of the fabricated droplet profile protruded structures (a) without and (b) with suction flushing.

The SEM images of the fabricated arrayed protruded structures are presented in Fig. 6. The height of each microstructure is 1 mm. The figure shows that the fabricated protruded microstructure using suction flushing offers no damaged tips, as shown in Fig. 6(b). Additionally, the whole arrayed microstructures haven't demonstrated any roundness or fillet at the microstructure root. Also, an orthogonal sidewall of each microstructure is observed in an array. In comparison, several protruded microstructure tips get damaged when machining is performed without suction flushing. It happened due to inadequate flushing at the central zone, resulting in higher-order discharges and arcing in the Reverse-µEDM process.

Quantitatively, MRR increased by approximately 25%, and a reduction in Tool-plate wear by 8% has been observed when machining is performed with suction flushing. The variation in both the responses is realized by the effective debris flushing from the machining area using suction-assisted flushing technology. Thus, the suction flushing technology could be benchmarked through a detailed investigation of various Reverse-µEDM responses and parametric studies.

6. Conclusion

In this study, a numerical model based on high-pressure suction-assisted flushing in the Reverse-µEDM process is introduced. The developed model analyzes the mechanism of debris evacuation from the narrow discharge gap through the suction flushing setup. The mechanism of debris distribution and flow-field behavior in the suction flushing is analyzed by DPM in ANSYS® using essential boundary conditions. Pilot experimental runs have been performed to validate the developed numerical model. Arrayed protruded microstructures in the droplet cross-sections have been fabricated with and without using suction flushing technology. An improvement in MRR by 25% and a reduction in Tool-plate wear by 8% approximately has been recorded for Reverse-µEDM with suction flushing. With this, it can be summarized that the implementation of high-pressure suction flushing technology enhances the performance of the Reverse-µEDM process. The enhancement is in terms of machining time and better surface qualities of fabricated 3D arrayed protruded microstructures. A detailed study of the process capabilities and design considerations for novel suction flushing setup will provide insights into future research direction.

References

[1] A. Tanveer et al., "Mechanism of Debris Ejection in Atomized Dielectric-Based Electric Discharge Machining," J of Micro and Nano Manuf., 2020; 8, 041017(1-6).

[2] S.A. Mastud et al., "Modeling debris motion in vibration assisted reverse micro electrical discharge machining process (R-MEDM)," J Microelectromech. Syst. 2015; 24(3), 661–676.
[3] H. Kishore et al., "Feasibility demonstration of µEDM for fabrication of arrayed micro pin-fins of complex cross-sections," J Manuf. Lett. 2020; 23, 14–18.
[4] M. Tanjilul et al., “A study on EDM debris particle size and flushing mechanism for efficient debris removal in EDM-drilling of Inconel 718,” J Mat Process Tech, 2018; 255, 263-274.
[5] T. Masuzawa et al., "Improved Jet flushing for EDM," CIRP Ann. Manuf. Technol., 1992; *41*(1), 239-242.
[6] Y. Wang et al. "Investigation of the effects of dielectric inlet pressure in inner jetted dielectric EDM milling", J Adv Mat Res, 2011; 189–193, 125–128.
[7] A. Pattabhiraman et al., "A Computational Model to Study Film Formation and Debris Flushing Phenomena in Spray-Electric Discharge Machining", J Micro Nano-Manuf, 2016; 4(3), 031002(1-10).
[8] S. Ndao et al., “Effects of pin fin shape and configuration on the single-phase heat transfer characteristics of jet impingement on micro pin fins,” J Heat Mass Trasnf, 2014; 70; 856-863.
[9] G. Karthikeyan et al, "A microscopic investigation of machining behavior in µeD-milling process", J Manuf Process, 2012; 14(3), 297–306.
[10] S.A. Mullya, S. A., "Accretion behavior and debris flow along interelectrode gap in µED-milling process", Int. J of Adv Manuf Technol, 2018; 96(9–12), 4381–4392.
[11] H. Kishore et al., “Assessment of process parameters and performance enhancement through a novel suction flushing technology in RµEDM”, Materials and Manufacturing Processes, DOI: 10.1080/10426914.2021.194805
[12] H. Kishore et al., "Modelling and simulation based surface characterization of reverse-µEDM fabricated micro pin-fins", Proc. CIRP. 2019; 81, 1230-1235.